

AUTOMATED DETECTION OF EXUDATES IN RETINAL IMAGES USING A SPLIT-AND-MERGE ALGORITHM

Hussain F. Jaafar, Asoke K. Nandi and Waleed Al-Nuaimy

Department of Electrical Engineering and Electronics
University of Liverpool, Brownlow Hill, Liverpool, L69 3GJ, UK
fax: +44 151 794 4540, email: {h.jaafar, a.nandi, wax}@liverpool.ac.uk, web: www.liv.ac.uk

ABSTRACT

Retinal image analysis is commonly used for the diagnosis and monitoring of diseases. In fundus photographs, bright lesions representing hard and soft exudates are the earliest signs of diabetic retinopathy. In this paper, an automated method for the detection of these exudates in retinal images is presented. Candidates are detected using a combination of coarse and fine segmentation. The coarse segmentation is based on a local variation operation to outline the boundaries of all candidates which have clear borders. The fine segmentation is based on an adaptive thresholding and a new split-and-merge technique to segment all bright candidates locally. Using a clinician's reference for ground truth exudates were detected from a database with 89.7% sensitivity, 99.3% specificity and 99.4% accuracy. Due to its distinctive performance measures, the proposed method may be successfully applied to images of variable quality.

Index Terms— Biomedical image processing, retinal images, exudate detection, local variation operator, split-and-merge technique.

1. INTRODUCTION

Diabetic-related eye diseases are the commonest cause of vision defects and blindness in the world. Monitoring the health of the retina is important for those people with signs of diabetic retinopathy (DR). Exudates are lipid leaks from blood vessels of abnormal retinas and are one of the most prevalent lesions at the early stages of DR [1]. Colour fundus images are used to detect exudates in retinal images. Fig. 1 shows a fundus image of an unhealthy retina with its main features and exudates.

Manual detection of exudates by ophthalmologists is laborious as they have to spend a great deal of time in the analysis and diagnosis of retinal photographs. Automated screening techniques for exudate detection have great significance in saving cost, time and labour. Image processing techniques for exudate detection can help in extracting the location, size and severity grade of exudates in the retinal images.

Several techniques for exudate detection have been proposed. Notable amongst these are those who utilised fuzzy C-means for segmentation in the different classification methods, such

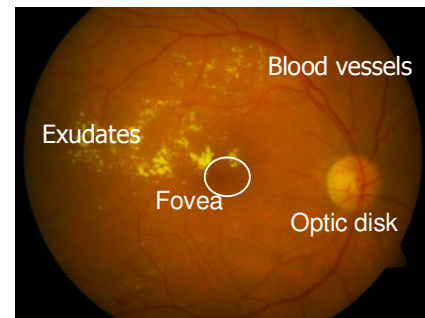


Fig. 1 – Retinal image with the main features and exudates.

as Sopharak *et al.* [2]. They employed morphological techniques for fine-tuning after the segmentation step and reported results of 87.28% sensitivity, 99.2% specificity. However, this method sometimes detects artefacts wrongly as exudates especially those resembling exudates. Xiaohui *et al.* [3] applied a hierarchical support vector machine to classify bright non-lesion areas. Kande *et al.* [4] incorporated spatial neighbourhood information into the standard FCM clustering for exudate classification. Osareh *et al.* [5] used an artificial neural network to classify segmented regions in term of lesion based classification with 93% sensitivity and 94.1% specificity. This method works well in LUV colour space, but the accuracy in case of uneven illumination is low.

Many other techniques have been proposed, such as Welfer *et al.* [6] who proposed a new method based on mathematical morphology for detecting exudates with sensitivity of 70.5% and specificity of 98.85%. However, the drawback of this approach is that it produces high misclassified portion for images that do not contain exudates. Sanchez *et al.* [7] proposed a method based on mixture models to threshold images in order to separate exudates from background. This method obtained a sensitivity of 90.2%. However, a limitation of this approach is that it sometimes fails to detect faint exudates. Garcia *et al.* [8] investigated three neural network classifiers to detect hard exudates: multilayer perceptron, radial basis function and support vector machine. Using a lesion-based criterion, they achieved a mean sensitivity of 88.14%. Sopharak *et al.* [9] employed naive Bayes and support vector machine classifiers for feature selection and exudate classification with 92.28% sensitivity and 98.41% accuracy, but both classifiers occasionally miss faint exudates.

This paper proposes an automated method for exudate detection in retinal images using a combination of segmentation procedures: coarse segmentation based on calculating the local variation for each pixel of the image and fine segmentation using an adaptive thresholding technique based on a new split-and-merge algorithm. Dynamic partitioning form (number and geometric shapes of partitions) are determined based on some features such as average intensities of the entire image and all sub-images, homogeneity in adjacent sub-images, standard deviation values and distribution of illumination throughout the image. Morphological operation is applied on the coarse and fine detection results to obtain the final segmentation of exudates. We base our work on dynamic parameter values since they enable our method to deal effectively with variable image qualities.

2. METHODOLOGY

The proposed method, which is free from user intervention, is designed to detect exudates in retinal images automatically. It uses a split-and-merge algorithm based on image features and a statistical hypothesis. This method includes four main stages; first the green component of the colour image is pre-processed to normalise and smooth the image and then eliminate the optic disk (Section 2.1). The second stage is coarse exudate detection using a local variation operator followed by classification making use of non-exudate features (Section 2.2). The third stage is fine exudate detection using an adaptive thresholding technique with dynamic image partitioning. Optimal partitioning is based on a split-and-merge algorithm (Section 2.3). The final stage is a combination of the two segmentation results using a morphological operation to obtain the final detection of exudates (Section 2.4).

2.1 Pre-processing and Optic Disk Elimination

Differences in luminosity, contrast, and brightness inside particular retinal image and among different retinal images make it difficult to extract retinal features and distinguish exudates from other bright features in images. So shade correction and noise removal are crucial tasks to prepare images for post-processing. To correct uneven illumination of images, a morphological top-hat operator with disk-shaped structuring element and fixed radius of 25 pixels was applied to the green component of the colour image. To reduce noise, a 3×3 median filter is applied to the shade corrected image. The bright optic disk can appear with similar features as exudates, and it is often identified incorrectly as an exudate; so it is essential to eliminate it before exudate detection steps. For this purpose, the method described in [10] has been followed to determine the centre and the radius information of the optic disk. In this method, a circular region of interest is found by isolating the brightest region of the image using morphological operations, and then the Hough transform is used to detect the main circular feature within the positive horizontal gradient image in this region of interest. The optic disk is masked by a disk with intensity value equal to the average intensity of the image. The input and output of the pre-processing and optic disk elimination steps are illustrated in Fig. 2.

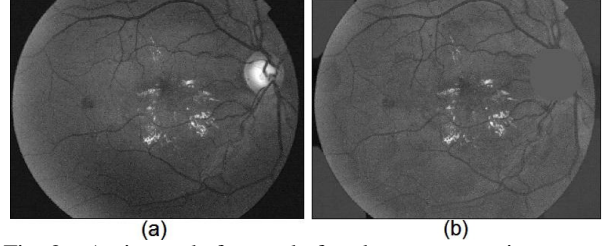


Fig. 2 – An image before and after the pre-processing operations, (a) green channel image, (b) pre-processed image.

2.2 Coarse Exudate Detection

Most of the images have non-uniform illumination. Fortunately most of the light reflection regions and artefacts do not have clear boundaries, while most exudates are characterised by having clear outlines in different degrees depending on the DR grade. One way to make use of this feature is to calculate the local variation for each pixel to get a standard deviation image. This image shows the main characterisation of the closely distributed clusters of exudates. Before applying the local variation operator, the high contrast blood vessels must be eliminated. Thus a morphological closing operator (ψ) was applied to the pre-processed image (G_1) with disk-shaped structuring element (ζ_1) of radius 6 pixels. The resulting image is denoted by G_2 as below:

$$G_2 = \psi^{\zeta_1} (G_1)$$

The image resulting from the local variation operator is denoted by G_3 as below:

$$G_3(x) = \frac{1}{N-1} \sum_{i \in w(x)} (G_2(i) - \mu(x))^2$$

where x is a set of all pixels in a sub-window $w(x)$, N is the number of pixels in $w(x)$, $\mu(x)$ is the mean value of $G_2(i)$ and $i \in w(x)$. The selection of window size is relied on the preferred compromise between the sensitivity and precision performance measures. So as the window size is larger the small exudates are more difficult to be detected leading to low sensitivity. Based on the experimental tests, we found that a window size of 9×9 gives good results.

In order to remove the objects in the standard deviation image, which have low local variation, automatic thresholding was applied using Otsu's thresholding method [11]. A morphological dilation operator (D), with a disk-shaped structuring element (ζ_2) of radius 3 pixels, was applied on the segmented image to ensure that the majority of neighbouring pixels are included in the candidate region. Then a morphological clear border operator (C) was applied to suppress structures that are lighter than their surrounding and connected to the image border. The coarse exudate detection result is denoted by G_4 as below:

$$G_4 = C(D^{\zeta_2} [T_\alpha(G_3)])$$

where T is the thresholding operator with automatic level (α). In order to classify non-exudates and then exclude them, the coarse segmented objects were discriminated using features,

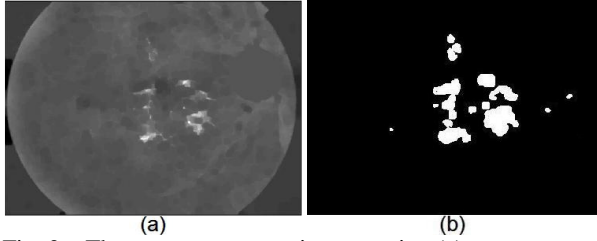


Fig. 3 – The coarse segmentation operation (a) pre-processed image with closing operator, (b) coarse segmented image.

such as major axis length, minor axis length, area and solidity. These properties were utilised in such a way that some relations between them or some limits in their values were used to classify features of non-exudates. The properties might belong to long and narrow objects which are formed due to bright vessels that had not been successfully removed. The operations of this step converted the shade corrected image to a binary image. This binary image is considered as the coarse white regions that outline the boundaries of all bright candidates which have clear borders. Fig. 3 shows the input and output images of the coarse segmentation step.

2.3 Fine Exudate Detection

Image binarisation using a global thresholding performs fast segmentation, but mostly results in undesired binary results especially when the input images are uneven or of poor quality. Consequently, adaptive local thresholding methods are used to get better segmentation results. However these methods have the disadvantage of slow running speed due to the re-computing operation of threshold value to each local region. In this paper the fine exudate detection is based on a combination of global and local thresholding. Local thresholding is applied to non-uniform background images by partitioning the image into dynamic number of geometric shapes (square and/or rectangle) of sub-images. The number and geometric shapes of the sub-images depend on image uniformity and the distribution of shade and bright locations throughout the image. Global thresholding is then applied to each uniform sub-image using histogram-based thresholding. This stage consists of two steps: the first step is to investigate the optimal number and directions of image partitioning using a split-and-merge algorithm. The second stage is to apply global thresholding on each individual sub-image separately with appropriate threshold value using a histogram-based thresholding.

2.3.1 Split-and-Merge Algorithm

Region-based segmentation algorithms can be classified into pure merging, pure splitting and split-and-merge schemes [12]. In the first scheme the image is divided into small regions which are then merged to form larger regions based on homogeneity criteria. The pure split algorithms view the entire image as an initial segmentation and then successively split each segment into quarters until a homogeneity state is reached. The split-and-merge scheme is based on partitioning the image into square sub-regions until homogeneity is verified. Then a merging process is applied to neighbouring sub-regions that satisfy some uniformity criterion.

In the proposed method we apply a split-and-merge technique, where the image is divided into square and/or rectangular partitions based on image features and a statistical hypothesis. In order to obtain the best number of partitions (as small as possible) for homogeneous sub-regions, the method traces the distribution of illumination throughout the image to separate shady and bright locations according to their levels and areas. In this stage the green channel component image is used after optic disk elimination, blood vessels removing, dark background surrounding the retina excluding and smoothing but without shade correction. The main disadvantage of applying shade correction is that the retinal image may sometimes have large abnormal areas which may lead to unexpected change in shading. The following steps describe briefly the split-and-merge procedures.

1. *Average intensity*: calculate the average intensity of the entire image described above.

2. *Image Partitioning*: select two variables $n_1=1, \dots, 6$ and $n_2 = 1, \dots, 6$ to be used in dividing the image into K different partitioning forms, where $K=n_1 \times n_2$. These 36 partitioning forms sometimes have same number and geometric shapes of sub-regions but with different locations on the entire image.

3. *Standard deviation*: for every one of the 36 partitioning forms, calculate the average intensities of all sub-images, and then the standard deviation based on average intensity of the entire image. Hence, we will have 36 values of standard deviation (σ_K , for $K= 1, \dots, 36$) for the 36 partitioning forms.

4. *Optimal partitioning*: it is divided into two steps:

Step1: Primitive partitioning: starting from the smallest number of partitions ($n_1=1, n_2=1$) ascending to the highest number of partitions ($n_1=6, n_2=6$), compare the standard deviation of each form with the maximum. A partitioning form with standard deviation equal to or greater than ninety percent of the maximum is selected empirically as the primitive partitioning form as below:

$$\sigma_{k(\text{selected})} \geq 0.9\sigma_{k(\text{max})}$$

Step 2: Merging homogeneous sub-images: in order to perform optimal adaptive thresholding and reduce processing time of segmentation, the number of uniform sub-regions should be as small as possible. Thus it is essential to investigate homogeneity of adjacent sub-regions to remerge them and get the optimal partitioning form. Homogeneity of any two sub-regions, say X with elements (x_1, x_2, \dots, x_m) and Y with (y_1, y_2, \dots, y_n) , is assessed by testing X and Y under an assumption of equality in their standard deviation σ_X and σ_Y . As a rough rule we can empirically consider the condition of equal standard deviation met if ratio of that larger to the smaller sub-region is less than 2. A statistical pooled t-test procedure is performed to decide the homogeneity of the adjacent sub-regions, where the hypothesis $H_0: X=Y$ (refers to the homogeneity state) is supposed. The significance level (β) is decided (we decided it to be 5%), and then values of degree of freedom (df) and test statistic (t) are calculated based on the information of adjacent sub-regions. The preceding parameters are used in the statistical t_α -table to estimate the probability of observing a value (p -value) which determines the final decision. If $p \leq \beta$, H_0 is rejected, otherwise the hypothesis is right.

2.3.2. Histogram-based Thresholding

Histogram-based thresholding may give imprecise result when the amount of overlap of the feature distribution in the histogram is large. Two methods have been used to rectify this problem [12]: first by applying the histogram-based thresholding to uniform local sub-images, and second by recursive application of the global method to increasingly fine-gained regions. In our method the uniform illumination locality is achieved by partitioning the image into uniform sub-images. Hence uniform illumination images are easy to be segmented as their histograms will be bi-modal distribution and the pixel intensities are clustered around two groups. Based on the result of optimal image partitioning gained in the preceding section, histogram-based thresholding was applied to the locations of sub-images of the smoothed green component channel (G_5) to obtain the fine segmentation of the image. Let a partition (P) of the image be defined as a subset of G_5 with respect to uniform lighting criterion. Hence running a global thresholding (T) throughout the image with variable threshold values (α) depending on the individuality of each sub-image can be represented by G_6 as below:

$$G_6 = \sum_{l \in k} T_{\alpha_l}(P_l)$$

The input and output of the fine segmentation is shown in Fig. 4.

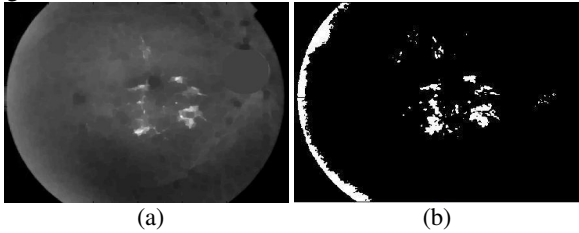


Fig. 4—The operation of fine segmentation (a) pre-processed green component image, (b) fine segmented image.

2.4 Final Detection of Exudates

Due to light reflection and bright vessels, the segmentation result often contains some non-exudates. Thus a combination of the coarse and fine images is used to improve the results. The final segmented image (G_7) is accomplished by applying a logical intersection operator on the coarse and fine segmentation results as below:

$$G_7 = G_4 \cap G_6$$

The coarse segmented image classifies pixels of the fine segmented image in such a way that candidates which have clear border can only be segmented as final exudates. Fig. 5 shows the inputs and output of the combination stage.

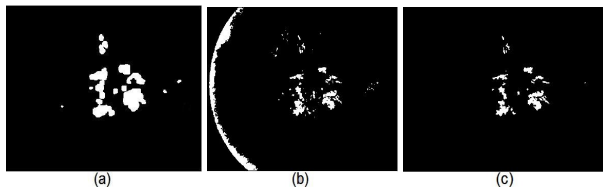


Fig. 5 – The results of the three stages (a) coarse segmentation (b) fine segmentation (c) final detection of exudates.

3. RESULTS AND DISCUSSION

Many experiments have been performed on normal and abnormal retinal images to test and validate our method.

140 images from different databases were used as below:

- 89 images from the DIARETDB1 database of resolution 1500×1152 with their clinician marked images [13] were used to validate our method at the pixel level. 47 of these images contain exudates while the remaining 42 either contain other type of lesions or are normal.
- 17 images with hard exudates and their clinician ground truth images from the Messidor database [14] of resolution 640×480 were used to validate the proposed method at the pixel level.
- 34 normal images from the Drive database [15] with resolution of 565×584 were used to measure the accuracy of the proposed method based on its ability to distinguish between normal and abnormal images.

Performance of the proposed method was assessed quantitatively by comparing the results with clinician hand-labelled data. Four types of pixels are considered in the method evaluation: True Positive (TP), False Positive (FP), False Negative (FN) and True Negative (TN). These quantities were computed with each individual processed image and utilized to measure the performance measures; sensitivity, specificity and accuracy. The proposed method was validated using 64 images (47 from DIARETDB1 and 17 from Messidor databases) with their clinician hand-labelled images in the pixel level with 89.7%, 99.3%, 99.4% sensitivity, specificity and accuracy respectively. Seventy-six images without hard exudates (35 from Drive and 42 from DIARETDB1 databases) were used to evaluate the proposed method at image-based classification, and the accuracy was 97.7%. Table 1 shows a comparison between the performance measures of the proposed method and some related works using DIARETDB1 database. Table 2 shows a comparison between the performance measures of the proposed method and some distinctive related works with different databases.

Table 1

Comparison of performance with DIARETDB1 databases.

Reference	Sens.%	Spec.%	Acc.%	Test set
Kande <i>et al</i> [4]	86	98	---	47
Welfer <i>et al</i> [6]	70.48	98.84	---	47
Proposed method	89.3	99.3	99.4	47

Sens. = Sensitivity, Spec. = Specificity, Acc. = Accuracy.

Table 2

Comparison of performance with different databases.

Reference	Sens.%	Spec.%	Acc.%	Test set
Osareh <i>et al</i> [5]	93	94.1	---	67
Garcia <i>et al</i> [8]	88.14	92.6	97	67
Sopharak <i>et al</i> [9]	92.28	98.52	98.41	39
Proposed method	89.7	99.3	99.4	64

Sens. = Sensitivity, Spec. = Specificity, Acc. = Accuracy.

A comparison between the proposed method and the clinician hand-labelled results is illustrated in Fig. 6.

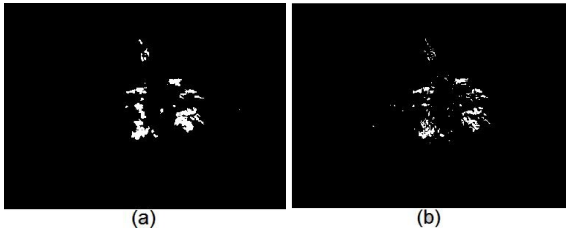


Fig. 6 – Exudate detection resulted by (a) the proposed method (b) the clinician hand-labelled (ground truth).

A comparison between the fine segmentation (shown in Fig. 5(b)) and the final detection of exudates (shown in Fig. 5(c)) demonstrates that the proposed coarse segmentation has played an important role in refining the fine segmentation results.

The ROC curve of our algorithm is shown in Fig. 7, and illustrates a compromise between the desired pixels (TP) and undesired pixels (FP) by changing the parameters of threshold and statistical significance levels.

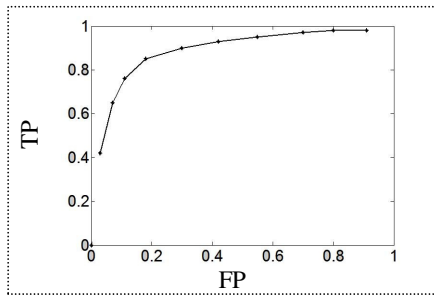


Fig. 7 ROC curve of the performance for various parameters.

4. CONCLUSIONS

The proposed method is adapted to deal with different types and qualities of images through taking all image information into account. The performance of the proposed method was measured against clinician hand-labelled images. Comparing with some recent related works, the proposed method indicates an improvement in the specificity and accuracy measures and reasonable sensitivity particularly with the high performance method in [9]. The performance results, demonstrated in this work, indicate that automated processing methods that are based on split-and-merge algorithm can give very competitive results in exudate detection. The strength of the proposed method comes from using computed parameters based on analysis of the image. A limitation in our work is that it occasionally fails to exclude some non-exudate objects particularly those that have similar features to real exudates.

5. ACKNOWLEDGEMENTS

The authors would like to thank DIARETDB1 Database Center [13], the Center of Mathematical Morphology, Mines Paris Tech. [14] and the Drive Database Center [15] for their co-operation in providing retinal images. Hussain F. Jaafar would like to acknowledge the financial support of the Iraqi government for this research.

REFERENCES

- [1] D. S. Fong *et al.*, “Diabetic Retinopathy”, *Diabetes Care*, vol. 26, no. 1, pp. 226-229, 2003.
- [2] A. Sopharak, and B. Uyyanonvara, “Automatic Exudates Detection from Non-dilated Diabetic Retinopathy Retinal Images Using Fuzzy C-means Clustering”, *Sensor*, vol. 9(3), pp. 2148-2161, 2009.
- [3] Z. Xiaohui and O. Chutatape, “Detection and Classification of Bright Lesions in Color Fundus Images”, *IEEE International Conference on Image Processing (ICIP)*, vol. 1, pp.139-142, 2004.
- [4] G. Kande, P. Subbaiah and T. Savithri, “Segmentation of Exudates and Optic Disk in Retinal Images”, *IEEE Sixth Indian Conference on Computer Vision, Graphic & Image Processing*, 2008.
- [5] A. Osareh, M. Mirmehdi, B. Thomas and R. Markham “Automated identification of diabetic retinal exudates in digital colour images”, *Ophthalmol*, vol. 87, pp. 1220-23, 2003.
- [6] D. Welfer, J Scharcanski, D. R. Marinho, “A coarse-to-fine strategy for automatically detecting exudates in color eye fundus images”, *Computerized Medical Imaging and Graphics*, CMIG-975, 2009.
- [7] C. I. Sanchez, M. Garcia, A. Mayo, M. I. Lopez and R. Hornero, “retinal image analysis based on mixture models to detect hard exudates”, *Medical Image Analysis*, v. 13, pp. 650-658, 2009.
- [8] M. Garcia, C. I. Sanchez, M. I. Lopez, D. Abasolo and R. Hornero, “Neural network basad detección of hard exudates in retinal images”, *Computer Methods and Programs in Biomedicine*, vol. 93, pp. 9-19, 2009.
- [9] A. Sopharak, M. N. Dailey, B. Uyyanonvara, S. Barman, T. Williamson and K. T. Nwe, “Machine learning approach to automatic exudate detection in retinal images from diabetic retinopathy”, *Journal of Modern Optics*, pp. 1-12, 2009.
- [10] S. Sekhar, W. Al-Nuaimy, and A. K. Nandi, “Automated Localization of Retinal Optic Disk Using Hough Transform”, *ISBI 2008, France*, pp. 1577-1580, 2008.
- [11] N. Otsu. “A Threshold Selection Method From Gray-Level Histograms”, *IEEE Trans. Systems, Man, and Cybernetics*, vol. 9(1), pp. 62-66, 1979.
- [12] S. Y. Chen, W. C. Lin, “Split-and-Merge Image Segmentation Based on Localized Feature Analysis and Statistical Test”, *Graphical Models and Image Processing*, vol. 53(5), pp. 457-475, 1991.
- [13] T. Kauppi, V. Kalesnykiene, J. K. Kamarainen, L. Lensu, I. Sorri, A. Raninen, R. Voutilainen, H. Uusitalo, H. Kalviainen and J. Pietila, “DIARETDB1 diabetic retinopathy database and evaluation protocol”, *Technical report*, Faculty of Medicine, University of Kuopio, Finland, 2007.
- [14] T. Walter, J. C. Klein and P. Massin, “A Contribution of image processing to the diagnosis of diabetic retinopathy-detection of exudates in colour fundus images of the human retina”, *IEEE Trans. Med. Imaging*, vol. 21, pp. 1236-43, 2002.
- [15] J. J. Staal, M. D. Abramoff, M. Niemeijer, M. A. Viergever, and B. van Ginneken, “Ridge based vessels segmentation in color images of the retina”, *IEEE Transaction on Medical imaging*, vol. 23, pp. 501-509, 2004.